Journal of Photochemistry and Photobiology A: Chemistry 204 (2009) 200–208

Contents lists available at ScienceDirect

Journal of Photochemistry and Photobiology A: Chemistry

journal homepage: www.elsevier.com/locate/jphotochem

Effect of thickness of ALD grown TiO_2 films on photoelectrocatalysis

Mikko Heikkilä*, Esa Puukilainen, Mikko Ritala, Markku Leskelä

Laboratory of Inorganic Chemistry, Department of Chemistry, P.O. Box 55, FI-00014 University of Helsinki, Finland

ARTICLE INFO

Article history:
Received 19 December 2008
Received in revised form 19 March 2009
Accepted 26 March 2009
Available online 5 April 2009

Keywords:
TiO_2
ALD
Photoelectrocatalysis
PEC
Methylene blue

ABSTRACT

Atomic layer deposited TiO_2 films were used for photoelectrocatalysis for the first time. Films with different thicknesses were grown and comprehensively characterized by structural and photoelectrochemical techniques. Methylene blue was used as a model substance in photocatalytic and photoelectrocatalytic degradation studies. In both cases, degradation rate was observed to saturate above certain film thickness. The reason for saturation could not be explained by the electrical parameters alone, and it was suggested that film morphology and crystalline structure are of major importance in this case.

1. Introduction

Photocatalysis by titanium dioxide is an advanced oxidation process widely studied in recent decades in, for example, water and wastewater purification [1]. Basics of photocatalytic process have been covered in several review articles [2–8]. In short, when semiconductor material is irradiated with photons of energy greater than or equal to the bandgap energy of semiconductor, valence band holes and conduction band electrons are formed. These electron–hole pairs then either migrate to the surface and participate in redox reactions or recombine on their way. The oxidative power of the holes and the hydroxyl radicals that are formed is the key to the photocatalytic degradation of harmful substances. Usually photocatalysis is done with particle slurries which makes the catalyst removal very difficult. By immobilizing the particles to surfaces, this drawback can be circumvented but at the same time the reactive surface area is significantly diminished. Another drawback in photocatalysis is the recombination of the generated electron–hole pairs. This can be reduced, e.g. by adding electron scavengers in the electrolyte [9], precipitating noble metals on photocatalyst surface [3] or by making composite structures [10]. The most efficient way to reduce the recombination and enhance the photocatalytic process is to separate the charges by applying an electric field across the immobilized TiO_2 layer. This process is usually referred as photoelectrocatalysis.

Photoelectrochemical splitting of water by TiO_2 was demonstrated already in early 1970s by Fujishima and Honda [11]. Photoelectrocatalytic destruction of organics was first reported by Vinogdopal et al. [12] followed shortly by Kim and Anderson [13]. Photoelectrochemical disinfection of water was first reported by Butterfield et al. [14]. Reviews concentrating on photoelectrocatalysis alone are rare but Egerton and Christensen have written a couple [15,16]. Rajeshwar et al. discuss the subject to some extent in their recent review on heterogeneous photocatalysis of organic dyes [8].

The effect of layer thickness on photocatalysis has not been studied much. In addition, the reported optimum thicknesses vary a lot and most of the studies have been done with sintered particles instead of dense layers. Photoelectrocatalytic studies of this kind are even more scarce with only few publications during the last decade [17,18]. The aim of this study was to investigate the effect of TiO_2 film thickness on photoelectrocatalytic degradation of commonly used model substance methylene blue. ALD was used to deposit the films since it provides excellent thickness control and produces very dense and uniform layers necessary for this kind of study [19]. In addition to photocatalytic degradation studies, the films were characterized in detail to further understand the effect of thickness on degradation rate.

2. Experimental

TiO_2 films were grown from $Ti(OMe)_4$ (Aldrich, 95%) and water in a flow type F120 ALD reactor (ASM Microchemistry Oy, Helsinki, Finland) using a process described earlier by Pore et al. [20]. 5 cm × 5 cm borosilicate glass and indium tin oxide (ITO) covered glass were used as substrates. Prior to the deposition the substrates were cleaned ultrasonically first in ethanol and then in deionised

* Corresponding author. Tel.: +358 9 191 50216; fax: +358 9 191 50198.
E-mail address: mikko.j.heikkila@helsinki.fi (M. Heikkilä).

1010-6030/$ – see front matter © 2009 Elsevier B.V. All rights reserved.
doi:10.1016/j.jphotochem.2009.03.019

water, after which they were rinsed with water and 50% ethanol and dried with N_2.

The ALD reactor was operated at about 10 mbar pressure. Nitrogen (made on site by Schmidlin NG3000 generator, rated purity of 99.9995%) was used as a carrier gas and for purging between precursor pulses. The titanium precursor was evaporated from an open boat at 130 °C inside the reactor. Water was held at room temperature in an external reservoir and was led into the reactor through needle and solenoid valves. Precursor pulse lengths were 0.5 and 0.6 s N_2 purges were applied in between. Films with six different thicknesses were deposited at 325 °C.

Transmittance spectra of the films grown on borosilicate were measured with a Hitachi U-2000 spectrophotometer in a wavelength range of 190–1100 nm. Film thicknesses and refractive indices were determined by fitting the measured transmission spectra [21].

Film crystallinity and phase was determined with a PANalytical X'Pert PRO MPD X-ray diffractometer using Cu Kα-radiation. Grazing incidence X-ray diffraction (GIXRD) measurements were performed using a Göbel mirror and 0.18° parallel plate collimator, and the incident angle was 1°. XRD measurements were also performed in the Bragg–Brentano configuration using automatic divergence and antiscattering slits set to 10 mm irradiated length. PIXcel detector was used for both geometries. Film morphology was studied with a Hitachi S-4800 field emission scanning electron microscope (FESEM). For AFM studies a Veeco Instruments Multimode V with Nanoscope V controller was used. Samples were measured in tapping mode in air using phosphorus-doped silicon probe (RTESP) delivered by Veeco Instruments. Several scans were performed from different parts of the samples to check the uniformity of the surface. Final images were measured from a scanning area of 2 μm × 2 μm with a scanning frequency of 0.5 Hz and no image processing except flattening was made. Roughness values were calculated as root-mean-square values (R_q).

Photoelectrochemical measurements, except for photocurrent spectra, were performed with an Autolab PGSTAT20 potentiostat using a three electrode setup with Pt as a counter electrode and 3 M Ag/AgCl as a reference electrode (Metrohm 6.0733.100). All potentials mentioned hereafter are related to this electrode. TiO_2 coated ITO was used as the working electrode. Active areas of the working and counter electrodes were about 20 cm^2. 120 ml of 0.1 M KCl aqueous solution was used as the electrolyte. Linear sweep voltammograms were measured towards anodic direction with a scanning speed of 10 mV/s. For photocurrent measurements, films were irradiated through the substrate with a 20 W black light (GE F20T12-BLB) that emits wavelengths 340–410 nm with a peak maximum at 365–370 nm. Intensity of the radiation was 1.5 mW/cm^2 at the substrate.

The photocurrent spectra were measured using a 300 W Xe lamp (Oriel 6259) as an irradiation source, and the wavelength was selected using a monochromator (Oriel 77700). The potential of the working electrode was set to +0.6 V using an Autolab PGSTAT100 potentiostat.

Electrochemical impedance spectroscopy was conducted using Solartron SI1286 electrochemical interface and Solartron SI1250 frequency response analyzer. The sample studied by EIS was a 160 nm TiO_2 layer grown on top of electron beam evaporated platinum. The platinum substrate was chosen instead of ITO in order to have only one oxide layer and therefore a simpler system to model. The impedance was recorded at constant polarization that was varied in 0.1 V steps between −0.4 and +0.8 V. The potential was let to stabilize for 15 min before each measurement. The impedance was measured as the current response to a superimposed sinusoidal voltage signal of 15 mV amplitude in a frequency range of 0.3–65,535 Hz. The equivalent circuit was fitted to the data using the ZPlot software supplied together with the Solartron equipment.

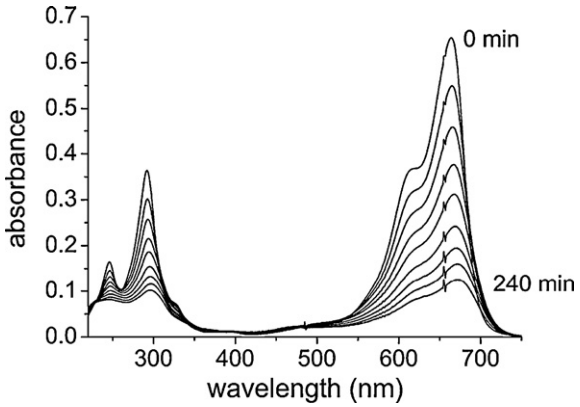

Fig. 1. Absorbance spectra of methylene blue in different stages of photoelectrocatalysis using 520 nm TiO_2 biased to +0.6 V vs. 3 M Ag/AgCl.

Aqueous solution of methylene blue (MB, $C_{16}H_{18}N_3Cl$, Oy Rohdoskeskus Ab) was used as a model substance for photocatalytic and photoelectrocatalytic degradations. MB was dissolved in 0.1 M KCl to give an initial MB concentration of 0.01 mM. The reactor was kept in dark for 1 h before starting the degradation study. During this time the solution was continuously bubbled with air in order to saturate the solution with oxygen that is necessary for photocatalytic degradations. The concentration change of MB during degradation was followed by measuring the value of absorbance maximum at 665 nm as a function of irradiation time with an HP 8453 spectrophotometer.

3. Results

3.1. Photocatalysis and photoelectrocatalysis of methylene blue

The absorbance spectra of MB in different stages of photoelectrocatalytic (PEC) degradation are shown in Fig. 1. The absorbances of all the four peaks decrease as a function of the degradation time which indicates that MB is being fully mineralized and no major by-products are formed.

The decrease of MB absorbance maximum at 665 nm as a function of degradation time is shown for photocatalysis (PC) and PEC in Fig. 2. The exponential decrease is observed especially for

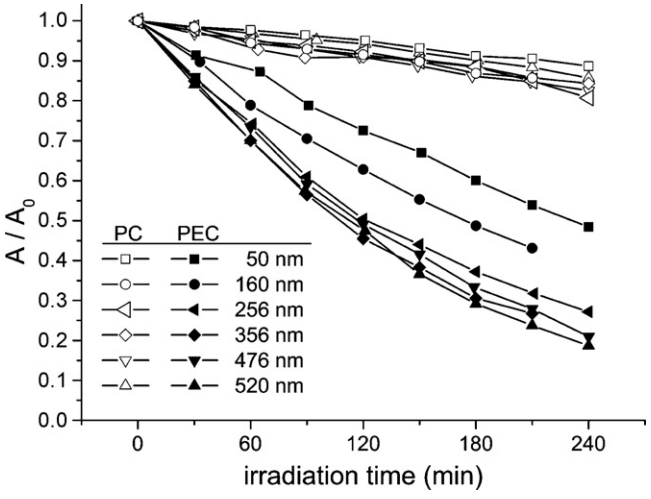

Fig. 2. The effect of film thickness on photocatalytic and photoelectrocatalytic degradation. Absorbance of methylene blue is related to initial value as a function of irradiation time. Films were biased to +0.6 V vs. 3 M Ag/AgCl during photoelectrocatalytic degradation.

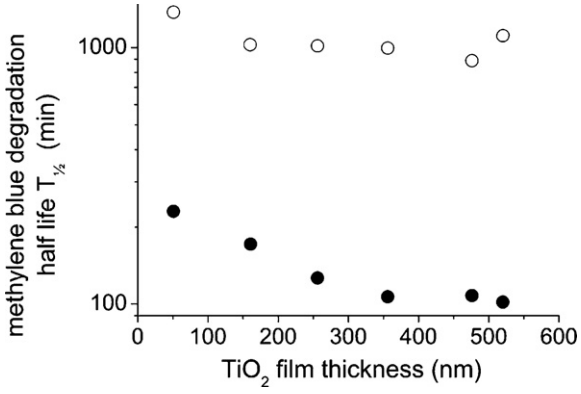

Fig. 3. Methylene blue degradation half lives for photocatalysis (hollow spheres) and for photoelectrocatalysis (solid spheres).

PEC, which suggests first-order kinetics. According to equation $-\ln(A/A_0) = kt$, a straight line can be fitted to the data and the apparent first-order rate constants k are acquired from the slope. The half life for MB degradation is acquired using equation $T_{1/2} = \ln 2/k$ and is depicted for both PC and PEC in Fig. 3. PC degradation rate stays quite constant above a film thickness of 150 nm whereas PEC degradation rate increases as a function of film thickness until it saturates at approximately 350 nm. The difference between PC and PEC degradations is huge, half lives being 22 h for PC and slightly less than 2 h for PEC.

3.2. Optical and structural properties

TiO_2 films grew consistently with a rate of approximately 0.6 Å/cycle and their average refractive index at 580 nm was 2.49. Both results are in good agreement with the results of Pore et al. [20]. Absorption constants α of the films were calculated from the transmission spectra according to Ref. [22]. Band gap values were then determined by plotting $(\alpha h\nu)^{1/2}$ vs. $h\nu$, where h is Planck's constant and ν is the frequency of the incoming radiation, and fitting a straight line to the linear part of the plot [23]. The band gap is obtained from the intercept of energy axis at $\alpha = 0$ as shown in Fig. 4 for a 476 nm thick TiO_2 film in which case a band gap of 3.30 eV was acquired. On average, optically measured band gap was 3.33 ± 0.05 eV for all the films, which is slightly higher than the anatase bulk value 3.2 but in good agreement with previous studies [20]. The blue shift of the TiO_2 film band gap caused by quantum confinement in thin layers has been thoroughly explained in a recent publication by King et al. [24].

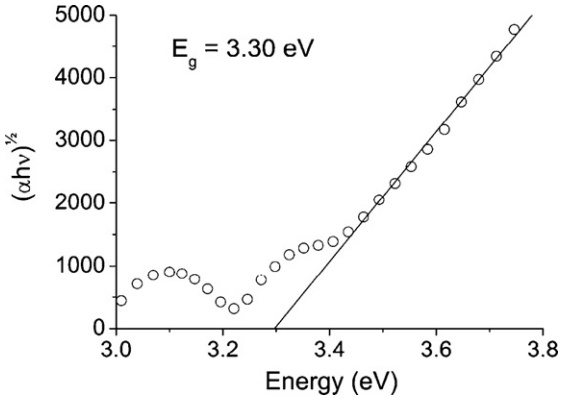

Fig. 4. A linear fit to the straight part of the $(\alpha h\nu)^{1/n}$ vs. $h\nu$ plot (Tauc plot) intercepts the energy axis at the optical band gap energy.

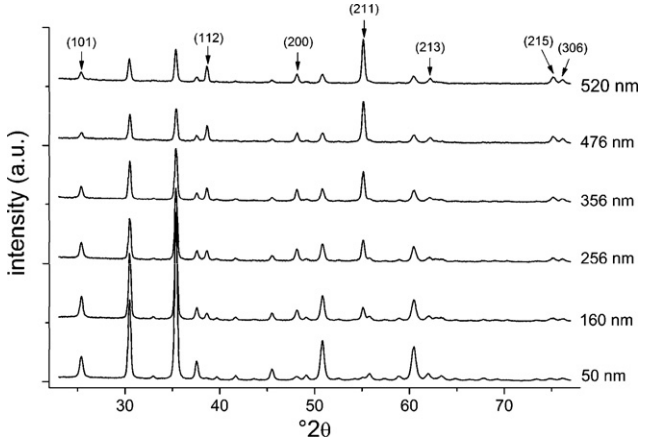

Fig. 5. Grazing incidence X-ray diffractograms of the deposited TiO_2 films. Indexed peaks are for the anatase phase, the others from the ITO film.

Grazing incidence X-ray diffractograms of the TiO_2 films on ITO films are depicted in Fig. 5. Based on the powder diffraction database, all the films are polycrystalline anatase [25]. The relative intensity of the (1 0 1) reflection slightly decreases when the film thickness increases, (2 0 0) reflection first increases and then decreases, and the intensities of (2 1 3), (2 1 5) and (3 0 6) reflections slightly increase as a function of film thickness. However, the intensities of the (1 1 2) and (2 1 1) reflections increase considerably as the film thickness increases leading to very different relative intensities when compared to powder diffraction file.

As the relative intensity increase is the most distinct for the thickest film, a phi scan (rotation around the normal of the sample) was performed for that sample using the same 1° incident angle as in the GIXRD measurement. The intensity variation of the first four reflections was minor during the rotation (not shown here) which suggests that if there is some preferred orientation, it is in a form of fiber texture.

Relative intensity differences could be also attributed to asymmetric crystallite growth and therefore crystallite size analysis was performed. Because for the thickest films the full width at half maximum (FWHM) of the peaks approached the resolution limit of the GI setup, the analysis was done using the θ–2θ setup that has much better resolution. Diffractograms were measured for the same set of films and are depicted in Fig. 6. The relative intensity changes are roughly similar to GIXRD measurements, with the important exception of (2 2 0) reflection that was missing from GIXRD data

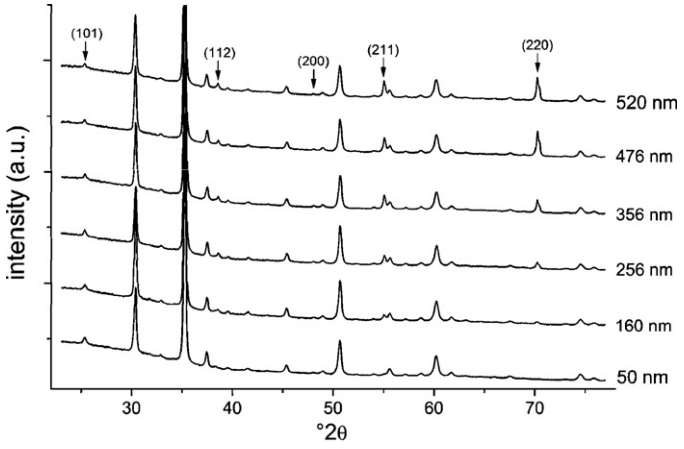

Fig. 6. θ–2θ X-ray diffractograms of the deposited TiO_2 films. Indexed peaks are for the anatase phase, the others from the ITO film.

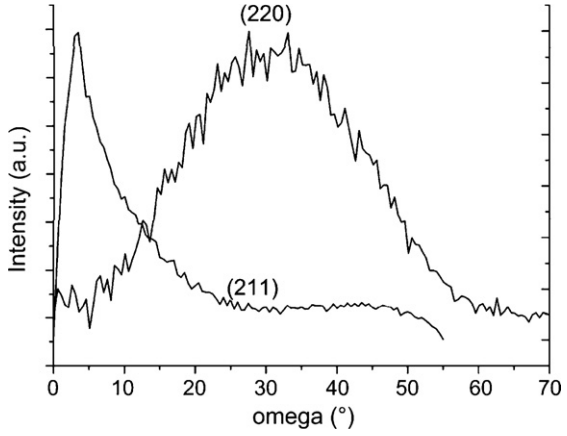

Fig. 7. Rocking curves over (2 2 0) and (2 1 1) reflections measured from 520 nm thick TiO_2 film.

and now is observed to have a clear thickness dependence. In order to further investigate possible preferential orientation in the films, rocking curves were performed for the first five reflections of the 520 nm film. While the other rocking curves were rather featureless, measurements on (2 2 0) and (2 1 1) reflections show clearly some orientation (Fig. 7). Rocking curve performed on (2 2 0) reflection has a large peak in the middle of the scan implying that the film is preferentially oriented in that direction, which is strongly supported by differences in GIXRD and θ–2θ diffractograms. For (2 1 1) there is a large peak in the beginning of the scan and small peak in the end, the former being overemphasized because of the larger irradiated area at small angles. This result is understandable since if (2 2 0) plane becomes predominant in the direction of the surface normal, (2 1 1) will be oriented very close to the direction observed in the rocking curves. This might also explain why the intensity of the (2 1 1) reflection increases strongly in GIXRD measurements.

Peak profile analysis was performed in order to find the FWHM of the reflections and these values were then used to calculate the apparent crystallite sizes using the Scherrer's equation. It has to be kept in mind that Scherrer's equation is not optimal for asymmetric crystallites because the Scherrer's constant can take broad range of values, that also depend on the reflection planes [26]. The crystallites were assumed to be spherical in this case and although the absolute value of the crystallite size is most likely incorrect, the trend of crystallite size growth seen in Fig. 8 can be considered quite reliable. As already observed in Fig. 6, the peak area of the (2 2 0) reflection increases strongly as a function of the film thickness and the crystallite size increases at the same time and it saturates above 356 nm. The peak area of the (2 1 1) reflection also increases but the continuous crystallite size growth slows down already after 160 nm.

Scanning electron micrographs of both film surfaces and cross sections are shown in Fig. 9. The underlying ITO film can be distinguished as slightly lighter colored area in most of the cross section images. As the film thickness increases the grains grow and surface roughness increases. From the micrographs one can observe that larger grains are frequently divided into parallel smaller grains. Atomic force microscopy was used to quantify the roughness and the AFM images are depicted in Fig. 10. The average grain size evaluated from SEM images and r.m.s. roughness evaluated from AFM images both increase in a same manner as seen in Fig. 11. The roughness is slightly less than 10 % of the grain size value increasing from 4.8 to 13.4 nm. The initial value is very close to the roughness measured from the ITO substrate, which is expected because of the conformal nature of the ALD process.

3.3. Electrochemical properties

Linear sweep photovoltammograms of all the films are shown in Fig. 12. The general shape of the voltammograms is approximately the same in all the films — sharp rise in photocurrent density around flat band potential is followed by a much slower growth. The maximum photocurrent density increases as a function of the film thickness and slows down beyond 356 nm.

Flat band potentials can be obtained from the voltammograms using the approximated Gärtner–Butler equation according to which a plot of I_{ph}^2 vs. V_b should be a straight line that intercepts the voltage axis at the flat band potential V_{fb} [23]. These fits are depicted in Fig. 13 and the flat band is -0.22 ± 0.02 V for all the films.

Photocurrent spectra are shown in Fig. 14. Films were irradiated either through the electrolyte–electrode (EE) interface or through the substrate–electrode (SE) interface. In the EE case all the films have the photocurrent spectra maximum at the same irradiation wavelength of about 300 nm. At lower wavelengths, the photocurrent is probably limited by the decreasing intensity of the lamp. In addition, the borosilicate window of the reactor vessel begins to absorb radiation when the wavelength is below 360 nm. The maximum of the photocurrent density increases as a function of film thickness approaching saturation above 356 nm.

The photocurrent densities are much smaller in the SE case because the radiation has to penetrate the borosilicate/ITO substrate before reaching the film. In this case the wavelength of the photocurrent density maximum is dependent of the film thickness: the thicker the film, the longer the wavelength of the maximum (Fig. 14). When the irradiation wavelength gets shorter,

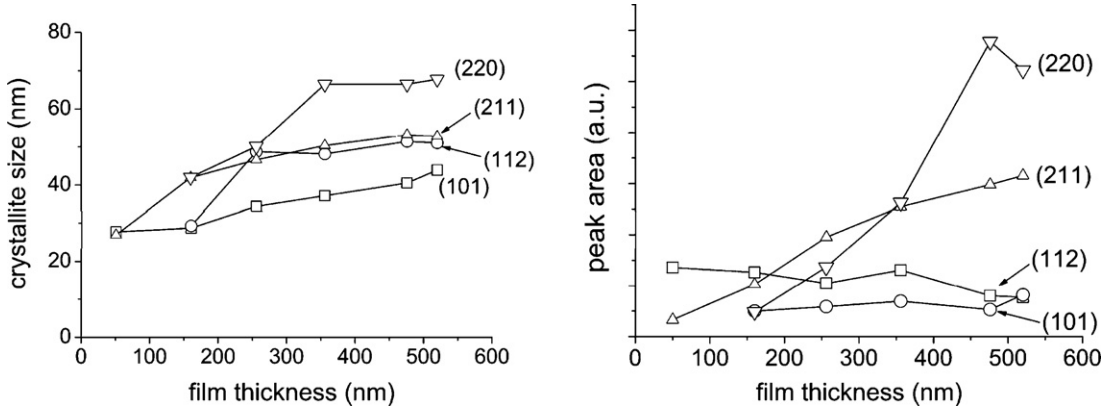

Fig. 8. Apparent crystallite sizes (left) and peak areas (right) for (1 0 1), (1 1 2), (2 1 1), and (2 2 0) reflections as a function of TiO_2 film thickness calculated from the θ–2θ scans.

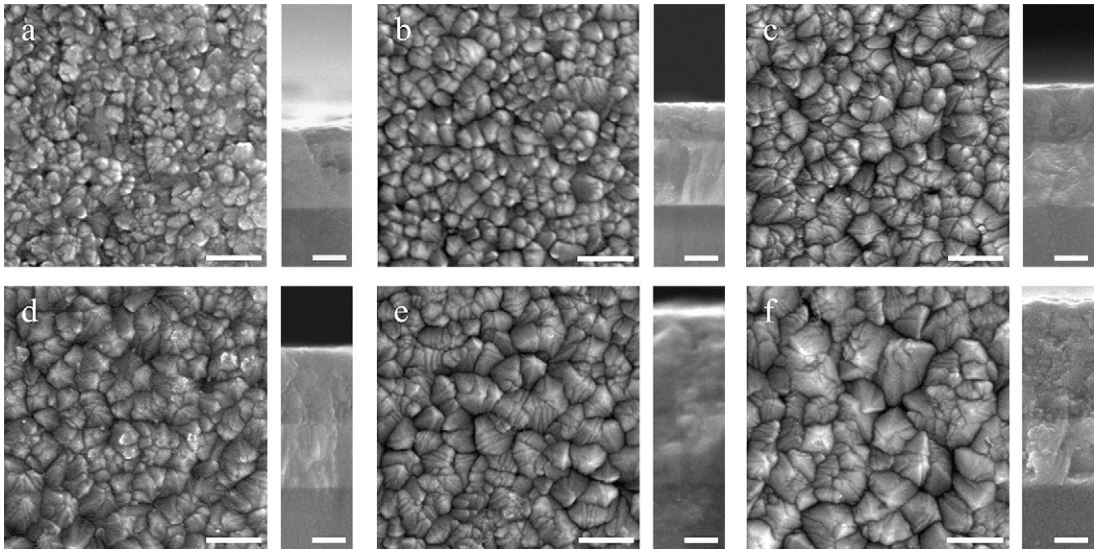

Fig. 9. Scanning electron micrographs of surfaces and cross sections of TiO_2 films: (a) 50 nm, (b) 160 nm, (c) 256 nm, (d) 356 nm, (e) 476 nm, and (f) 520 nm. Scale bar is 150 nm.

larger proportion of the radiation reaching TiO_2 is absorbed near the SE interface, and the probability of the generated hole to reach the EE interface gets smaller being smallest for the thickest film.

Based on the photocurrent spectra, the best performance in this setup could be achieved when thicker than 350 nm film was irradiated through the electrode–electrolyte interface with 300 nm wavelength irradiation. However, the spectral distribution peak

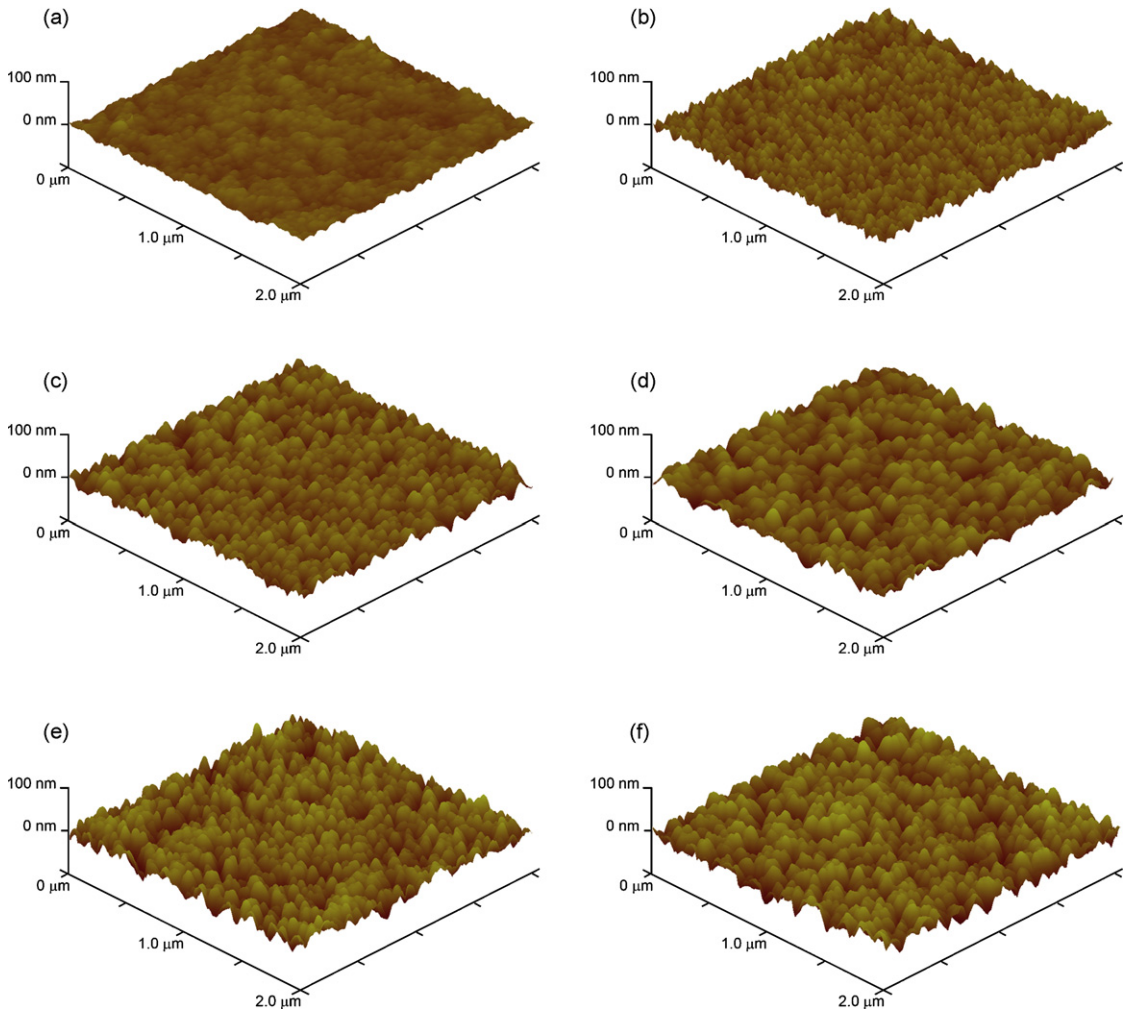

Fig. 10. AFM images of the deposited TiO_2 films: (a) 50 nm, (b) 160 nm, (c) 256 nm, (d) 356 nm, (e) 476 nm, and (f) 520 nm.

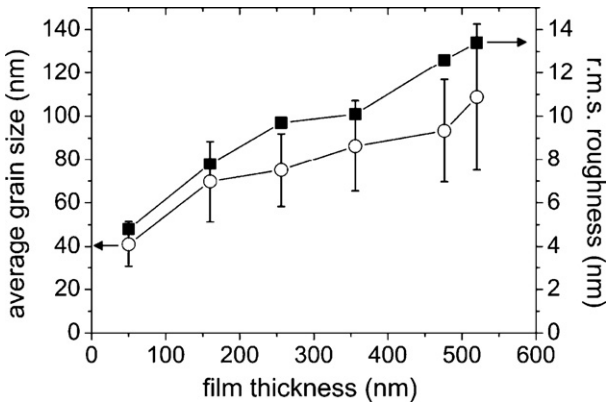

Fig. 11. Average grain size and TiO_2 film roughness as a function of film thickness.

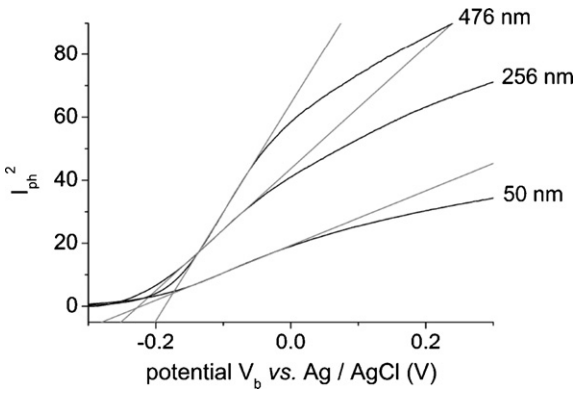

Fig. 13. Flat band determination from I_{ph}^2 vs. potential graphs for selected thicknesses.

of the lamp used in this study was around 365–370 nm. When photocurrent spectra are looked more closely around those wavelengths (bottom part of Fig. 14), the photocurrents are slightly higher for the SE irradiation.

Band gap can be calculated from the absorption threshold of the photocurrent spectra using the following relationship between photocurrent I_{ph} and irradiation energy $h\nu$

$$I_{ph} = A\frac{\left(h\nu - E_g\right)^n}{h\nu} \quad (1)$$

where $n = 0.5$ for direct and $n = 2$ for indirect optical transitions the latter being the case for TiO_2 [27]. By plotting $(I_{ph}h\nu)^{1/2}$ as a function of $h\nu$ allows the band gap to be obtained from the intersection between fitted straight line and energy axis. This is illustrated in Fig. 15 for 476 nm thick film. On average, the band gap calculated from photocurrent spectra was 3.38 ± 0.01 eV for all the films, which is slightly higher than the value obtained from the UV–vis transmittance spectra.

Fittings of the EIS data was made using the equivalent circuit that consists of parallel-coupled coating capacitance and pore resistance, and in series with the pore resistance there is also the parallel-coupled double layer capacitance and the charge transfer resistance. Frequency range used for fittings was 0.5–5000 Hz and χ^2 was less than 0.003 for all measured potentials. The well known Mott-Schottky equation is

$$\frac{1}{C_{sc}^2} = \frac{2}{\varepsilon_r\varepsilon_0 e N_D A^2}\left(V_B - V_{fb} - \frac{kT}{e}\right) \quad (2)$$

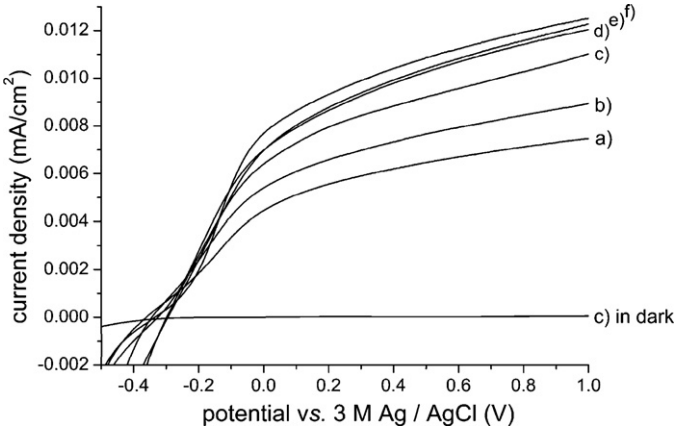

Fig. 12. Linear sweep voltammograms of UV irradiated (a) 50 nm, (b) 160 nm, (c) 256 nm, (d) 356 nm, (e) 476 nm and (f) 520 nm thick TiO_2 films. The dark current measured for 256 nm film is very close to zero.

where C_{sc} is the capacitance of the semiconducting layer, ε_r is the permittivity of the semiconductor, ε_0 the vacuum permittivity, N_D the donor density, A the electrode area, V_B the electrode potential and V_{fb} the flat band potential [23]. Using the capacitances acquired from EIS measurements, a Mott-Schottky plot was created (Fig. 16) and by fitting a straight line on the linear part of the plot, a flat band potential $V_{fb} = -0.61$ V was acquired. This value is approximately 0.4 V more negative than the one obtained from the voltammograms and could be attributed to photo-shift of the flat band potential [28,29]. The donor density can be calculated from the slope of the linear fit. In literature, the permittivity value for anatase is reported to be between 30 and 50 [30,31]. Using 40 as a permittivity, a donor density of $N_D = 2.8 \times 10^{25}$ m^{-3} is obtained.

4. Discussion

In photoelectrocatalysis the potential applied on TiO_2 electrode was clearly shown to accelerate the degradation of methylene blue when compared to photocatalysis. The degradation efficiency depends on film thickness both in PC and in PEC. In PC the degradation rate saturates above 150 nm film thickness, whereas in PEC the rate keeps increasing until 356 nm thickness is reached. Since there are few previous data on the effect of film thickness on PEC efficiency of dense TiO_2 layers, the comparison to literature is quite difficult. Hitchman and Tian used CVD grown titania for photoelectrocatalysis of 4-chlorophenol and found that with anatase films the degradation rate increases from 133 to 275 nm, remains constant between 275 and 698 nm and decreases above that thickness [17]. The saturation level is quite close to what we observed in the present study. Song et al. have investigated PC and PEC degradation of Rhodamine B using film thicknesses between 400 and 800 nm [18]. The films were prepared through hydrolysis of titanium tetrafluoride solution at 60 °C and subjected to heat treatment thereafter. They observed a PEC degradation rate maximum at 460 nm and the rate decreased rapidly at higher thicknesses. The PC rate on the other hand kept rising to 540 nm after which it saturated. The main difference to present study was that the films were irradiated from the electrolyte's side, which partly explains the different saturation values found in present study. Because of that and different thickness range in our research, we cannot readily compare these two studies. As explained by Song et al., the decrease of PEC efficiency after maximum might be related to increasing difficulties in electron migration to the back contact. However, the increase in PC efficiency at such high thickness has to be related to crystallinity and morphology as explained later. They also found out that the calcination of film improves the degradation efficiency and attributed this to increased crystallinity and DC conductivity of the calcinated films.

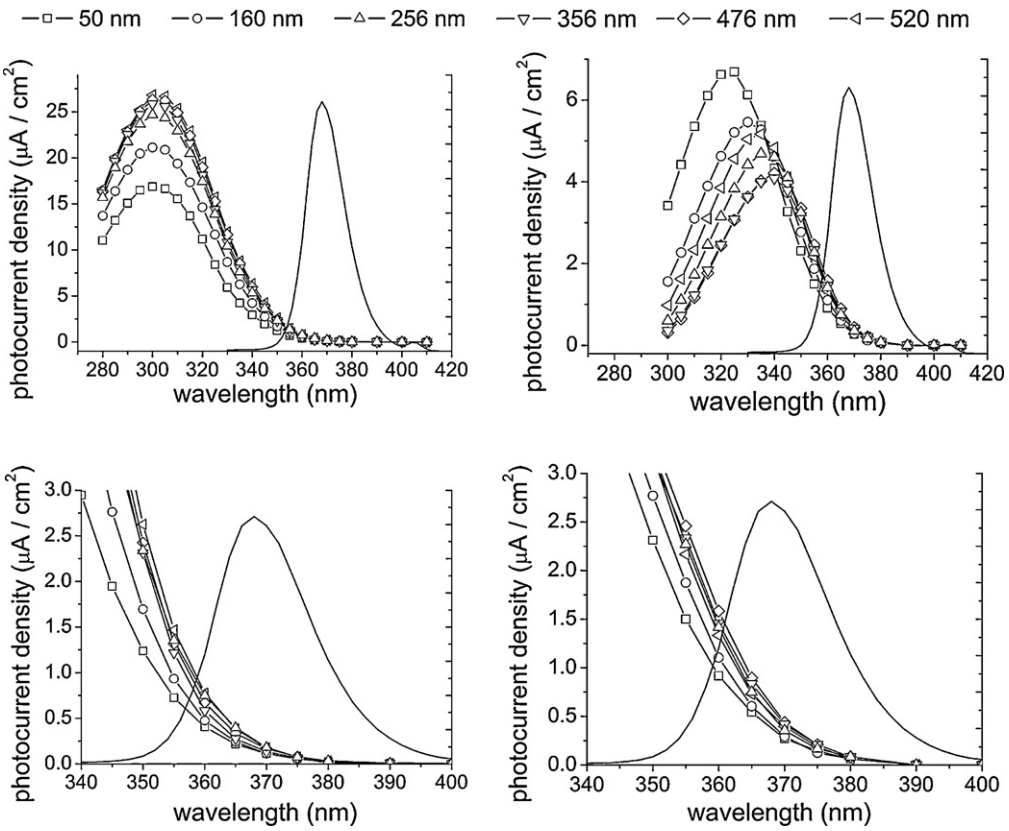

Fig. 14. Photocurrent spectras. Solid line without symbols is the spectrum of the UV lamp used in this study. Spectra on the left-hand side were measured with irradiation through the electrolyte–electrode (EE) interface and spectras on the right-hand side with irradiation through the substrate–electrode (SE) interface. Images at the bottom show the wavelength range 340–400 nm in greater detail.

In other MB PEC study Egerton et al. [32] found that PC is faster than PEC in above 0.1 mM concentration, probably due to the difficult adsorption of the positive MB molecule to the positive electrode surface. With the 0.01 mM concentration used in this study, however, PEC is much faster in degrading the MB molecules (Fig. 3). This indicates that PEC is very efficient in degrading even positively charged molecules, when the concentrations are not very high.

The physical parameters of the deposited TiO_2 films correspond to the values found in literature. Sene et al. [33] measured a flat band potential of −1.0 V for their sol–gel deposited films and Zanoni et al. [28] obtained −0.34 V for theirs. In both cases the flat band potential was determined from the onset of the photocurrent, and our value determined with the same technique was −0.2 V which is slightly more positive. When flat band potential was determined from the Mott-Schottky plot using the capacitance from the EIS data, Oliva et al. got values between −0.76 and −0.12 V [27], Radecka −0.36 and −0.2 V [34] and in their other study −0.6 V [35]. The last value is very close to the −0.61 V acquired in this study from the Mott-Schottky plot.

In the work of Radecka et al. flat band potentials and donor densities from several studies are gathered to one table [35]. While the flat band potentials are quite close to what we measured in the same pH range, there is a large scatter in the donor densities. As noted by Radecka et al., this is probably due to the different preparation methods and thermal treatments. The variation is between 4.7×10^{22} and 7.4×10^{26} m^{-3} and our result $N_D = 2.8 \times 10^{25}$ m^{-3} fits well within that range.

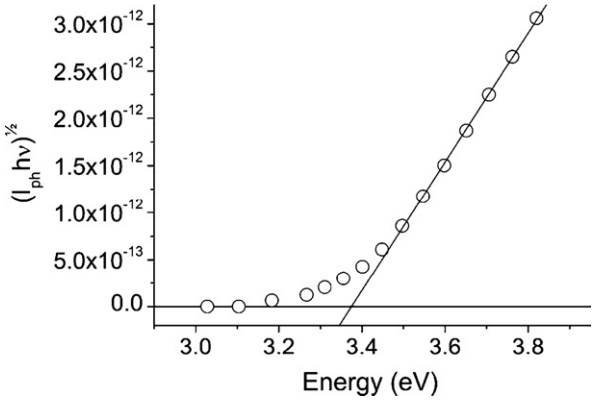

Fig. 15. Photocurrent spectra of 476 nm thick TiO_2 film. Band gap of 3.35 eV is obtained from the intersection of the linear fit with the energy axis.

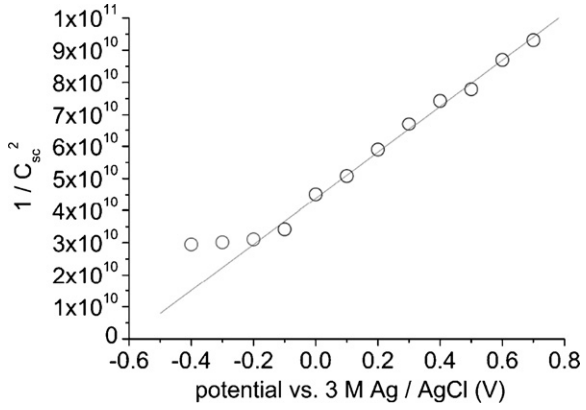

Fig. 16. Mott-Schottky plot of a 160 nm thick TiO_2 film on platinum substrate. Donor density $N_D = 2.8 \times 10^{25}$ m^{-3} is acquired from the slope and flat band potential −0.61 V from the potential axis intersect.

The depletion layer thickness can be calculated using Eq. (3) [29]:

$$W_D = \left(\frac{2\varepsilon_r\varepsilon_0}{eN_D}\right)^{1/2}\left(V_B - V_{fb} - \frac{kT}{e}\right) \quad (3)$$

Using the donor density obtained from the Mott-Schottky plot, for +0.6 V polarization the depletion layer is about 15 nm. Using the flat band potentials and donor densities collected by Radecka et al. [35], the depletion layer thickness varies from a few nanometers to few tens of nanometers, typically remaining below 50 nm expect for some films with very low donor concentration. Based on these estimates of depletion layer thickness and the minority carrier diffusion distance of approximately 100 nm [17], one would think that the optimal thickness of the film would be close to the sum of these two, a value between 100 and 200 nm. This is not the case in our study, though, since the PEC degradation rate begins to saturate above 350 nm thickness. Apparently there are more factors affecting the degradation rate besides thickness.

Grain boundaries are one factor leading to the recombination of charge carriers. It was shown that the crystallite size calculated from θ–2θ XRD measurements increases as a function of film thickness. This increase is faster for two most intense reflections and especially for (2 2 0) reflection that was also observed to be preferred orientation for these films. Since the measurement was θ–2θ, these results mean that the charge carrier's free path before grain boundary increases as the film thickness increases. It is very interesting to note that the crystallite size of the most intense reflection (2 2 0) saturates at the same thickness as the PEC degradation efficiency. Increasing crystallite and grain size might be the reason why we observe the highest degradation rate at higher than anticipated thickness. Depletion layer is probably better developed in larger crystallites and there are less recombination centers during hole's travel towards the electrode surface. In a very recent paper by Cheng and Chen [36], the authors have investigated the photoelectrochemical properties of atomic layer deposited TiO_2 films. They found out that increase in grain size and decrease in defect density have a remarkable effect on photocurrents which supports our findings in the present study. This could be further verified, e.g. by growing epitaxial TiO_2 films with different thicknesses so that there would be no disturbance from the grain boundaries.

5. Conclusions

The effect of ALD grown TiO_2 film thickness on photocatalytic and photoelectrocatalytic degradation rate of methylene blue was investigated. The degradation rate was observed to reach saturation as a function of thickness, in photocatalysis at 150 nm and in photoelectrocatalysis at 356 nm. In addition to degradation studies, films were characterized using voltammetry, photocurrent spectroscopy, EIS, XRD, FESEM and AFM. All the electrical parameters agreed well with the literature, but based on those values, the saturation thickness for PEC degradation seemed too high. XRD and film morphology measurements done in this study suggest that for polycrystalline films, certain crystallite and grain size is needed in order to produce a well defined depletion layer and less obstacles for hole diffusion leading to more efficient degradation.

References

[1] S. Parsons, Advanced Oxidation Processes for Water and Wastewater Treatment, IWA Publishing, London, 2004.
[2] M.A. Fox, M.T. Dulay, Heterogeneous photocatalysis, Chem. Rev. 93 (1993) 341–357.
[3] A.L. Linsebigler, G. Lu, J.T. Yates Jr., Photocatalysis on TiO_2 surfaces: principles, mechanisms, and selected results, Chem. Rev. 95 (1995) 735–758.
[4] A. Mills, S. Le Hunte, An overview of semiconductor photocatalysis, J. Photochem. Photobiol. A 108 (1997) 1–35.
[5] A. Mills, S. Lee, Semiconductor photocatalysis, in: S. Parsons (Ed.), Advanced Oxidation Processes for Water and Wastewater Treatment, IWA Publishing, London, 2004, pp. 137–166.
[6] N. Serpone, A.V. Emeline, Fundamentals in metal-oxide heterogeneous photocatalysis, in: M.D. Archer, A.J. Nozik (Eds.), Nanostructured and Photoelectrochemical Systems for Solar Photon Conversion, Imperial College Press, 2008, pp. 275–392.
[7] A. Fujishima, X. Zhang, D.A. Tryk, TiO_2 photocatalysis and related surface phenomena, Surf. Sci. Rep. 63 (2008) 515–582.
[8] K. Rajeshwar, M.E. Osugi, W. Chanmanee, C.R. Chenthamarakshan, M.V.B. Zanoni, P. Kajitvichyanukul, R. Krishnan-Ayer, Heterogeneous photocatalytic treatment of organic dyes in air and aqueous media, J. Photochem. Photobiol. C 9 (2008) 171–192.
[9] M. Hepel, J. Luo, Photoelectrochemical mineralization of textile diazo dye pollutants using nanocrystalline WO_3 electrodes, Electrochim. Acta 47 (2001) 729–740.
[10] I. Shiyanovskaya, M. Hepel, Bicomponent WO_3/TiO_2 films as photoelectrodes, J. Electrochem. Soc. 146 (1999) 243–249.
[11] A. Fujishima, K. Honda, Electrochemical photolysis of water at a semiconductor electrode, Nature 238 (1972) 37–38.
[12] K. Vinodgopal, S. Hotchandani, P.V. Kamat, Electrochemically assisted photocatalysis: titania particulate film electrodes for photocatalytic degradation of 4-chlorophenol, J. Phys. Chem. 97 (1993) 9040–9044.
[13] D.H. Kim, M.A. Anderson, Photoelectrocatalytic degradation of formic acid using a porous titanium dioxide thin-film electrode, Environ. Sci. Technol. 28 (1994) 479–483.
[14] I.M. Butterfield, P.A. Christensen, A. Hamnett, K.E. Shaw, G.M. Walker, S.A. Walker, C.R. Howarth, Applied studies on immobilized titanium dioxide films as catalysts for the photoelectrochemical detoxification of water, J. Appl. Electrochem. 27 (1997) 385–395.
[15] T.A. Egerton, P.A. Christensen, Photoelectrocatalysis processes, in: S. Parsons (Ed.), Advanced Oxidation Processes for Water and Wastewater Treatment, IWA Publishing, London, 2004, pp. 167–184.
[16] T.A. Egerton, P.A. Christensen, S.A.M. Kosa, B. Onoka, J.C. Harper, J.R. Tinlin, Photoelectrocatalysis by titanium dioxide for water treatment, Int. J. Environ. Pollut. 27 (2006) 2.
[17] M.L. Hitchman, F. Tian, Studies of TiO_2 thin films prepared by chemical vapour deposition for photocatalytic and photoelectrocatalytic degradation of 4-chlorophenol, J. Electroanal. Chem. 538–539 (2002) 165–172.
[18] X. Song, J. Wu, M. Yan, Photocatalytic and photoelectrocatalytic degradation of aqueous Rhodamine B by low-temperature deposited anatase thin films, Mater. Chem. Phys. 112 (2008) 510–515.
[19] M. Ritala, M. Leskelä, Atomic layer deposition, in: H.S. Nalwa (Ed.), Handbook of Thin Film Materials, Deposition and Processing, vol. 1, Academic Press, San Diego, 2002, p. 103.
[20] V. Pore, A. Rahtu, M. Leskelä, M. Ritala, T. Sajavaara, J. Keinonen, Atomic layer deposition of photocatalytic TiO_2 thin films from titanium tetramethoxide and water, Chem. Vap. Deposition 10 (2004) 143–148.
[21] M. Ylilammi, T. Ranta-aho, Optical determination of the film thicknesses in multilayer thin film structures, Thin Solid Films 232 (1993) 56–62.
[22] R. Swanepoel, Determination of the thickness and optical constants of amorphous silicon, J. Phys. E: Sci. Instrum. 16 (1983) 1214–1222.
[23] F. Di Quarto, S. Piazza, M. Santamaria, C. Sunseri, Photocurrent spectroscopy of thin passive films, in: H.S. Nalwa (Ed.), Handbook of Thin Film Materials, Characterization and Spectroscopy of Thin Films, vol. 2, Academic Press, San Diego, 2002, p. 373.
[24] D.M. King, X. Du, A.S. Cavanagh, A.W. Weimer, Quantum confinement in amorphous TiO_2 films studied via atomic layer deposition, Nanotechnology 19 (2008) 445401.
[25] Powder diffraction file, card 21–1272, JCPDS-ICDD, International Center for Diffraction Data, 1994.
[26] J.I. Langford, A.J.C. Wilson, Scherrer after sixty years: a survey and some new results in the determination of crystallite size, J. Appl. Crystallogr. 11 (1978) 102–113.
[27] F.Y. Oliva, L.B. Avalle, E. Santos, O.R. Cámara, Photoelectrochemical characterization of nanocrystalline TiO_2 films on titanium substrates, J. Photochem. Photobiol. A 146 (2002) 175–188.
[28] M.V.B. Zanoni, J.J. Sene, M.A. Anderson, Photoelectrocatalytic degradation of Remazol Brilliant Orange 3R on titanium dioxide thin-film electrodes, J. Photochem. Photobiol. A 157 (2003) 55–63.
[29] N. Sato, Electrochemistry at Metal and Semiconductor Electrodes, Elsevier, Amsterdam, 1998.
[30] H. Tang, K. Prasad, R. Sanjines, P.E. Schmid, F. Levy, Electrical and optical properties of TiO_2 anatase thin films, J. Appl. Phys. 75 (1994) 2042–2047.
[31] R. Mori, M. Takahashi, T. Yoko, Photoelectrochemical and photocatalytic properties of multilayered TiO_2 thin films with a spinodal phase separation structure prepared by a sol–gel process, J. Mater. Res. 20 (2005) 121.
[32] T.A. Egerton, H. Purnama, S. Purwajanti, M. Zafar, Decolouration of dye solutions using photoelectrocatalysis and photocatalysis, J. Adv. Oxidat. Technol. 9 (January (7)) (2006) 79–85.

[33] J.J. Sene, W.A. Zeltner, M.A. Anderson, Fundamental photoelectrocatalytic and electrophoretic mobility studies of TiO_2 and V-doped TiO_2 thin-film electrode materials, J. Phys. Chem. B 107 (2003) 1597–1603.
[34] M. Radecka, TiO_2 for photoelectrolytic decomposition of water, Thin Solid Films 451–452 (2004) 98–104.
[35] M. Radecka, M. Wierzbicka, M. Rekas, Photoelectrochemical cell studied by impedance spectroscopy, Phys. B Condens. Matter 351 (2004) 121–128.
[36] H. Cheng, C. Chen, Morphological and photoelectrochemical properties of ALD TiO_2 films, J. Electrochem. Soc. 155 (2008) D604–D607.